Analysis of the $Pb_{0.30}Ca_xSr_yTiO_3$ ternary system: The effect of Ca^{2+} and Sr^{2+} cations on the electrical properties of $PbTiO_3$

Amanda Fernandes Gouveia[1+], Lara Kelly Ribeiro[2], Marcelo Assis[2], Elson Longo[2], Juan Andrés[1], Fenelon Martinho Lima Pontes[3]

1. University Jaume I, Department of Physical and Analytical Chemistry, Castelló, Spain.
2. Federal University of São Carlos, CDMF, São Carlos, Brazil.
3. São Paulo State University, Department of Chemistry, Bauru, Brazil.

+Corresponding author: Amanda Fernandes Gouveia, Phone: +5534964728071, Email address: gouveiad@uji.es

ABSTRACT: Powder and thin films of the $Pb_{0.30}Ca_{0.10}Sr_{0.60}TiO_3$ (PCST 30/10/60) and $Pb_{0.30}Ca_{0.60}Sr_{0.10}TiO_3$ (PCST 30/60/10) ternary system were synthetized by the polymeric precursor method and the thin films deposited on the $Si/SiO_2/Ti/Pt$ substrate. The effects of the Sr^{2+} and Ca^{2+} cations substitutions on the electrical and structural properties of the $PbTiO_3$ were characterized by X-ray diffraction, Infrared, and Raman spectroscopy. Theoretical calculations were performed using the CRYSTAL06 program associated with the density functional theory and the B3LYP functional hybrid. Structural and electronic properties of the system were analyzed. The

band gap values calculated for the PCST 30/10/60 and PCST 30/60/10 models were 3.35 and 3.41 eV, respectively. The results showed an evolution to a greater symmetry in the direction to the cubic $SrTiO_3$ structure and the phase transition was characterized by the Curie temperature dependence. The broad bands above FE-PE phase transition temperature suggest a phase transition diffuse type. It is explained by a local symmetry disorder due to a higher Sr^{2+} and Ca^{2+} cations concentration in the $PbTiO_3$ host lattice.
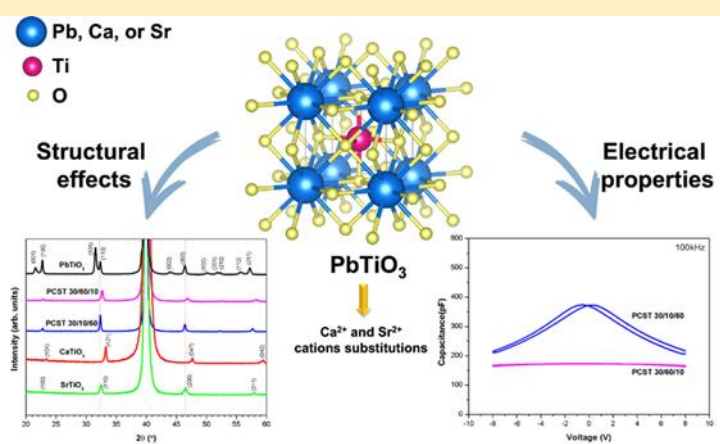
1. Introduction

Ferroelectric ceramics are among the several nanostructured materials (Yuan *et al.*, 2021; Zhang *et al.*, 2022). The idea that electronic information can be stored in the electrical polarization states of a ferroelectric material is known for a long time. Therefore the need for new information technologies, heavy incentive has been given to the development of materials and methods related to ferroelectric semiconductor memory devices by many countries and high-tech companies (e.g. Seiko Epson Corporation, Symetrix Corporation, IBM, Matsushita Electric, Sharp, Fujitsu, Ramtron International Corporation and many others) focused on the search for new materials that enable the evolution of current ones, or preferably, the creation of new technologies (Daglish and Kemmitt, 2000; Muller *et al.*, 2003).

Nanostructured ferroelectric memory systems are strong candidates for this mission due to the combination of several and interesting features in a single material (Y. Yang *et al.*, 2020). In recent years, these systems have been used in the form of nanostructured thin films. In particular, the dynamic random-access memory (DRAM) (Ling *et al.*, 2006), where the material is above the ferroelectric transition temperature or the ferroelectric random-access memory (FeRAM) (Crawford, 1971; Eshita *et al.*, 2014; 2018; Mao *et al.*, 2013), where in the ferroelectric state, below the ferroelectric transition temperature, the ability to reorient the polarization spontaneously has aroused its use as a nonvolatile memory element (Han *et al.*, 2013; Vopson and Tan, 2016). Consequently, these memories have expanded, being used in cell phones, digital cameras, electric vehicles, computers (notebooks or PCs), smart cards, etc. (Kim and Lee, 2006; Mao *et al.*, 2013). In this strategic market, there is also the possibility of using products such as identification data (ID) tag cards, where large information technology (IT) and telecommunications companies are involved. Among them, the Japanese company Matsushita Electric (best known for its Panasonic household product brand), Toshiba, IBM and others in the field stand out. These companies invest millions of dollars a year in the development and improvement of DRAM and FeRAM memories.

Surprisingly, the area of ferroelectric memories is relatively unexplored. However, this is a field of particular importance for developing knowledge and technologies related to the properties, and applications on a nanometric scale of ferroelectric memories. Among these materials, the one with a perovskite-type structure (ABO_3 composition) stands out with its high interaction with various metals substrates, insulators, and semiconductor industry (Kour and Pradhan, 2021; J. Lee, 1999).

The phenomenon of ferroelectricity in complex oxides of the ABO_3 perovskite-type can be controlled if the characteristic size of the crystal can also be controlled (at a certain critical size (J. Lee, 1999), ferroelectricity can even be suppressed) (Ahmadi and Araghi, 2021). Understanding the properties of ABO_3 films and their interrelationship at the nanoscale may be the basis for developing a new generation of devices that will allow for the long-awaited transition from microelectronics to nanoelectronics. The perovskite with the ABO_3 structure is composed by $[AO_{12}]$ and $[BO_6]$ clusters and, according to the material, can crystallize, for example, in a cubic, tetragonal and/or orthorhombic structure (Souza, 2021).

The interest in ferroelectric thin films, especially thin films based on lead (Pb), such as $PbTiO_3$ (PT) is motivated by its potential applications as nonvolatile ferroelectric memory devices, an application based on the long retention period of the polarization and low polarization fatigue (Lázaro *et al.*, 2005; C. Yang *et al.*, 2021). Both parameters are related to the degradation phenomenon strongly dependent on the preparation process (Zhao *et al.*, 2019).

Aiming at controlling the ferroelectric properties, the coupling between the properties of the PT, $CaTiO_3$ (CT) and $SrTiO_3$ (ST) perovskites opens new possibilities for data storage in DRAM's or FeRAM's elements, which can be prepared to maximize the memory capacity in a small volume. There are several publications that bring different combinations of PT, CT and ST perovskites, resulting systems as: $Pb_{0.90}Ca_{0.10}TiO_3$ (F. Pontes *et al.*, 2008), $Pb_{0.60}Ca_{0.20}Sr_{0.20}TiO_3$, $Pb_{0.50}Ca_{0.25}Sr_{0.25}TiO_3$ and $Pb_{0.40}Ca_{0.30}Sr_{0.30}TiO_3$ (D. Pontes *et al.*, 2014), $Pb_{0.60}Sr_{0.40}TiO_3$ (Leal *et al.*, 2004), $Pb_{0.74}Ca_{0.26}TiO_3$ (Capeli *et al.*, 2017), $Pb_{0.76}Ca_{0.24}TiO_3$ (D. Pontes *et al.*, 2001a; b), and $Pb_{0.50}Sr_{0.50}TiO_3$ (F. Pontes *et al.*, 2005).

To achieve the great potential of $Pb_{0.30}Ca_xSr_yTiO_3$ (PCST) thin films (formed from the combination of PT, CT and ST perovskites) for applications in DRAM or FeRAM semiconductors, one should know how to synthesize these materials and control the stability of the perovskite phase during its processing. In this paper, it was proposed to fix the Pb^{2+} cations concentration in 0.30 and use different concentration of Ca^{2+} and Sr^{2+} cations to obtain distinct PCST ternary systems from that found in the literature.

2. Methods

2.1 Experimental procedure

The procedure for synthesizing powder and thin films of $Pb_{0.30}Ca_{0.10}Sr_{0.60}TiO_3$ and $Pb_{0.30}Ca_{0.60}Sr_{0.10}TiO_3$ (abbreviated as PCST 30/10/60 and PCST 30/60/10, respectively) consisted of producing a polymeric resin using the soft chemistry method known as polymeric precursor route. Details of the preparation method can be found in literature (Longo *et al.*, 2004; D. Pontes *et al.*, 2001a; F. Pontes et al., 2003; 2004). The resin was burned at 400 °C for 4 h at a heating rate of 5 °C min^{-1} to form a powder. The power was characterized by X-ray diffraction (XRD) and by Raman-spectroscopy to verify the incorporation of the Ca^{2+} and Sr^{2+} cations in the PT host matrix. The ferroelectric thin films were deposited on $Si/SiO_2/Ti/Pt$, using spin-coating process at 6500 rpm for 30 s, and crystallized in conventional oven in a two-stage heat treatment carried out as follow: initial heating rate of 5 °C min^{-1} until reach 400 °C and maintained for 4 h in an oxygen atmosphere to pyrolyze the organic material, followed by heating at 700 °C for 2 h at a heating rate of 5 °C min^{-1} in the same atmosphere for crystallization. Measurements of dielectric and ferroelectric properties were taken in the $Au/thin\ films/Pt/Ti/SiO_2/Si$ multilayer structure configuration. Regarding the measurement of electrical properties, circular top Au electrodes were prepared by evaporation through a shadow mask with a 4.9×10^{-2} mm^2 dot area to obtain an array of capacitors. The deposition was conducted under vacuum down to 10^{-6} torr. The frequency dependence of the capacitance was measured by an Agilent 4294A Precision Impedance Analyzer in the frequency ranging from 100 Hz to 10 MHz. The capacitance–voltage (C–V) curves were obtained using an Agilent 4294A Precision Impedance Analyzer with an AC signal of 50 mV$_{rms}$ at 100 kHz; all measurements were taken at 25 °C.

Temperature-dependent capacitance measurements of thin films were taken from 10 to 300 K using a closed-cycle helium cryostat and a G^w Instek LCR 819 meter for capacitance measurements; all measurements were performed at 100 kHz. For these measurements, circular Au electrodes with an area of approximately 4.9×10^{-2} mm^2 were deposited (using a shadow mask) by evaporation on the heat-treated film surfaces which served as top electrodes in an $Au/thin\ films/Pt/Ti/SiO_2/Si$ configuration.

2.2 Theoretical procedures

Theoretical calculations of electronic structure ab-initio level for the studied PCST ternary systems were performed using the CRYSTAL06 program (Dovesi *et al.*, 2005), associated with density functional theory (DFT) and the B3LYP functional hybrid (Becke, 1993; C. Lee *et al.*, 1988). The XCrySDen (2019) program was used to draw the density of states of each atom models.

The experimental results shown that the PCST ternary systems present a local organization toward to the cubic ST structure. Therefore, from the unit cell of cubic ST optimized structure, expansions in the z-axis were made to simulate a supercell, where the percentages of cations could be simulated accurately. The structural and electronic properties of these materials were analyzed to corroborate the experimental results.

3. Results and discussion

To verify the formation of the PCST ternary systems the XRD analysis was performed for the powder, as illustrated in Fig. 1. From the results, it is possible to affirm that the incorporation of Sr^{2+} and Ca^{2+} cations in the PCST ternary system was effective, obtaining a pure phase without the presence of one or more intermediate stages or even other phases, like PT, CT, ST, $Pb_xCa_yTiO_3$, or $Pb_xSr_zTiO_3$.
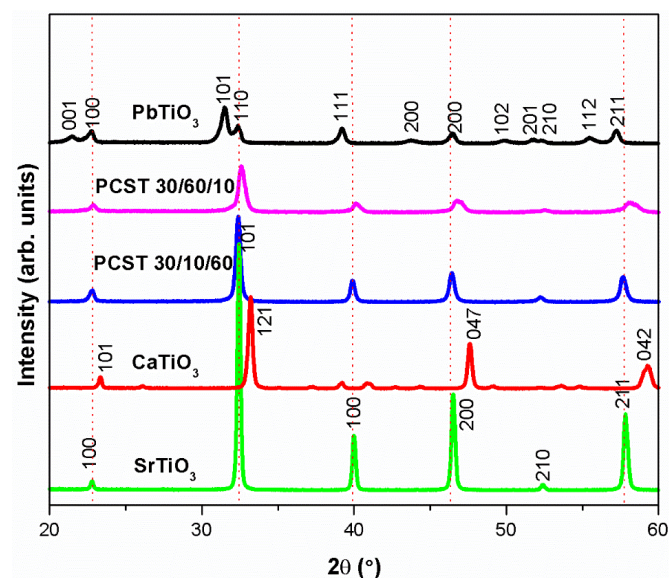
Figure 1. XRD pattern of the powder of PCST30/10/60, PCST30/60/10, PT, CT, and ST heat treated at 700 °C.

It is observed that the PCST ternary systems have evolved to a higher symmetry, in this case, toward a cubic ST structure. However, there are still weak diffraction peaks observed in the system PCST 30/60/10, which correspond to the diffraction planes of PbTiO₃.

From the PIKFIT program, the lattice parameters were calculated for each system based on the tetragonal structure (Tab. 1). Table 1 also shows the parameters obtained from the DFT calculations. The data show that there is a distortion in the structure, changing from tetragonal to cubic, by increasing the Sr^{2+} cations concentration in the system, as there is a decrease in the parameter c, which indicates the tetragonality factor, while the parameter remains practically unchanged. The same result was theoretically obtained using the CRYSTAL06 program, confirming the data obtained experimentally.

Table 1. Lattice parameters (Å) for ternary systems.

Sample	Experimental			Theoretical		
	a	*c*	*c/a*	*a*	*c*	*c/a*
PCST 30/10/60	3.9117	3.9122	1.000	3.8938	3.8918	0.999
PCST 30/60/10	3.8756	3.8880	1.003	3.8789	3.8771	0.999

To corroborate data of XRD analysis, the micro-Raman spectroscopy was performed. Figure 2 illustrates the micro-Raman spectra for the PCST ternary systems and for the PT standard system as reference. It is possible to observe a decrease in the tetragonality by the overlap of the micro-Raman modes E(1LO)/A1(1TO) and B1+E/A1(2TO) with the incorporation of the Sr^{2+} and Ca^{2+} cations into the PT system. The E(1TO) soft mode decreases to lower wavelength and tends to complete disappearing, indicating a change of symmetry of a tetragonal to cubic system.
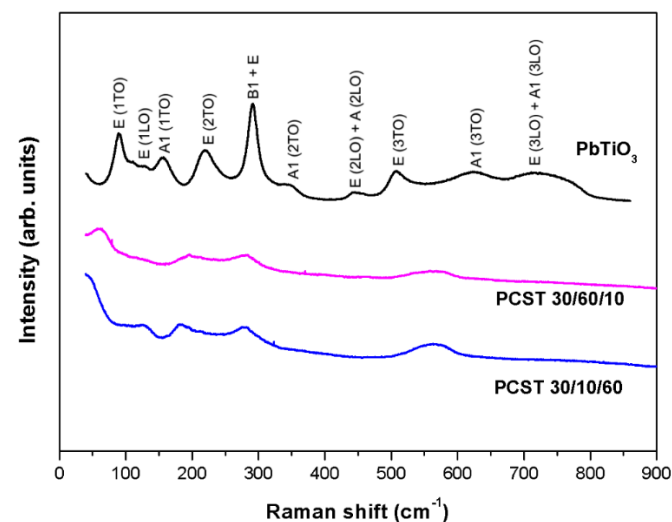
Figure 2. Micro-Raman spectra for PbTiO₃, PCST30/10/60, and PCST30/60/10 systems.

The micro-Raman spectrum for PCST 30/60/10 system was also analyzed for different temperatures between 20 and 500 °C (Fig. 3). This study aimed at investigating the behavior of micro-Raman bands as the temperature increases, as well as to search for signs of structural changes.
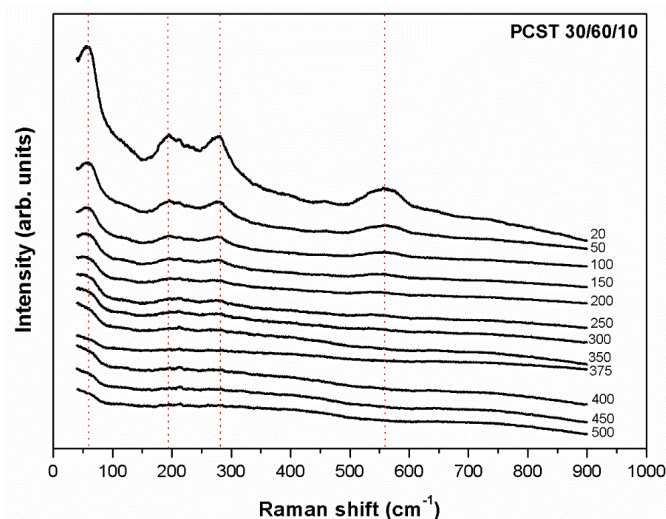
**Figure 3.** Micro-Raman spectrum for powder of PCST30/60/10 ternary system as function of the temperature.

It is well-known that the active micro-Raman modes E(1TO) and A1(1TO) for pure PT, and in particular the E(1TO) mode are soft modes, which are directly related to the transition from tetragonal to cubic type.

The phase transition temperature can be determined by micro-Raman spectroscopy by observing the temperature in which the soft mode disappears. Thus, Fig. 4 reveals that there was no phase transition from tetragonal to cubic, as the soft mode did not disappear with the increase of temperature, there is only an enlargement of the E(1TO) mode. An alternative for this case is an analysis as a function of pressure, i.e., to study the phase transition by applying hydrostatic pressure to the sample inside a diamond cell. Another solution is to prepare thin films of this composition and investigate its electrical properties at low temperature, for example,

from 10 to 300 K to check if a certain phase transition temperature exists.

For the analysis of the PCST ternary systems in powder form and after confirming the Ca^{2+} and Sr^{2+} cations incorporation in the system without the formation of second phase, the thin films were then prepared and characterized.

Figure 4 illustrates the XRD pattern for the thin films of the PCST ternary systems, as well as the PT, CT and ST structures.
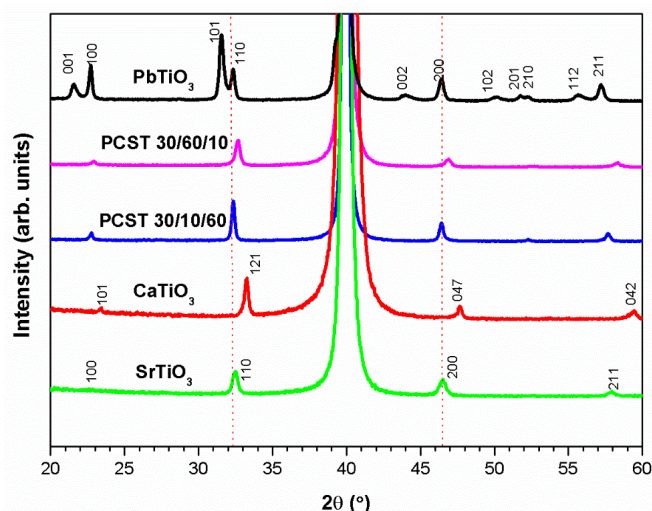
Figure 4. XRD pattern of the thin films of PCST 30/10/60, PCST 30/60/10, PT, CT, and ST on Si/SiO$_2$/Ti/Pt substrate heat treated at 700 °C.

Figure 4 allows to affirm that the replacement of the Pb^{2+} cations by Ca^{2+} and Sr^{2+} cations at the A site ([AO$_{12}$] clusters) caused a drastic change in the XRD patterns of the PT structure. All thin films have a polycrystalline nature. Therefore, the striking tetragonal characteristic of the PCST ternary system thin film disappeared due to the substitution in the [AO$_{12}$] cluster, as can be seen by comparing it with the PT standard.

The lattice parameters were also calculated (Tab. 2). The XRD pattern of the samples are very similar to the pure ST system, proving the complete replacement of Ca^{2+} and Sr^{2+} cations in the Pb site, mainly for the Sr^{2+} cations, as also observed in the PCST powder. Therefore, it is deduced that the Sr^{2+} cations are responsible for the transition from a tetragonal to a cubic phase; otherwise, an orthorhombic phase or even a mixture of phases would be observed. So, it can be assumed that the effect of substitution of Pb by Ca^{2+} cations is less pronounced than the effect of its substitution by Sr^{2+} cations at the [AO$_{12}$] clusters since it presents a very similar XRD pattern to ST structure. This effect can be caused by the change in the type of bond involved, now between Sr^{2+} and Ca^{2+} cations, where Sr^{2+} cations will form a bond with a much higher ionic character (with radial characteristic) than Ca^{2+} cations. This difference in bond type is a determining factor for these structural changes. Moreover, it may have a system tending to stabilize a more symmetrical structure.

Table 2. Lattice parameters for the PCST ternary systems thin films. The cubic system was considered for all PCST thin films.

Sample	Structure	Parameters	Special group
*PbTiO$_3$	Tetragonal	$a = b = 3.899(0)$	P4mm
		$c = 4.153(0)$	
*CaTiO$_3$	Orthorhombic	$a = 5.3796(1)$	Pbnm
		$b = 5.4423(3)$	
		$c = 7.6401(5)$	
*SrTiO$_3$	Cubic	$a = b = c = 3.905$	Pm3m
PCST 30/60/10	Cubic	$a = b = c = 3.877$	Pm3m
PCST 30/10/60	Cubic	$a = b = c = 3.910$	Pm3m

Note. The unit of the parameters (a; b; c) are in Å; *data extracted from JCPDS forms.

To corroborate the XRD data the infrared spectroscopic response was analyzed with reflectance accessory. Figure 5 shows the reflectance spectra for thin films, as well as standards for SrTiO$_3$ and CaTiO$_3$ systems. These standards are important to clearly confirm the evolution to a structure with very similar characteristics of SrTiO$_3$.

As can be seen in Fig. 5, there is a similarity between the spectra of thin films and ST, assuming three infrared active modes for the cubic structure, much more than that for the system CT, in which the mode identified by *c* is not present in any sample of PCST thin films (Tab. 3).

The spectra showed well-defined bands and characteristics of a crystalline material. The bands in the region between 400–1000 cm^{-1} are due to the longitudinal (LO) and transverse (TO) optical modes, which are associated with the crystallinity of the material (Liu *et al.*, 2010; F. Pontes *et al.*, 2002; 2003). These absorption bands obtained by the reflectance technique in the infrared spectrum are caused by the excitation of

optically active vibrations. The main band observed for the different compositions of PCST thin films located in the 600–800 cm^{-1} region is characterized by the stretch vibration of the Ti−O bond (metal-oxygen in the [TiO$_6$] clusters). The bands in the shorter wavelength region can be attributed to Pb−O, Ca−O or Sr−O stretch vibrations.
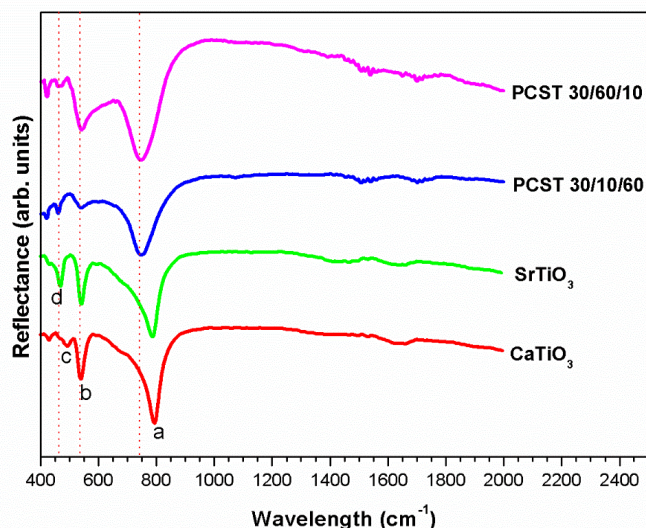
Figure 5. FT-IR reflectivity spectra for CaTiO$_3$, SrTiO$_3$, PCST30/10/60, and PCST30/60/10.

In the FT-IR spectrum obtained by reflectance, changes in vibrational modes and their displacements are indications of structural evolution, i.e., change from a tetragonal phase to a pseudo cubic, cubic, or orthorhombic phases. Therefore, the vibrational analysis of these materials revealed some changes in vibrational modes. These changes occurred both in displacement level and in the band width of vibrational modes. Thus, the substitution at A-site in the PT structure corresponds to a change in the distances of the A−O and/or Ti−O bonds, and this substitution is responsible for the large coupling effect in the higher energy bands.

The difference between the ST and CT spectra for the PCST systems and their similarity to ST suggest that the [TiO$_6$] clusters present greater symmetry for the PCST system in both compositions. The simplicity of this qualitative analysis suggests that the octahedral environment at site Ti is symmetrical, not reflecting large distortions to the tetragonal or orthorhombic structure, which could be responsible for the polarization, that is caused by the presence of permanent dipoles within the material.

After confirming the effective incorporation of Ca^{2+} and Sr^{2+} cations at A-site into the PT structure, forming PCST ternary system, the nanostructured thin films were characterized for their dielectric and ferroelectric properties.

Table 3. FT-IR frequencies modes for the ST, CT, and PCST thin films.

System	a	b	c	d
SrTiO$_3$	786.84	541.92	-	468.63
CaTiO$_3$	794.56	539.99	493.70	430.06
PCST30/60/10	747.31	541.92	460.92	422.35
PCST30/10/60	746.34	541.92	461.88	420.42

Figure 6 illustrates the dielectric capacitance results in function of the frequency for the PCST 30/60/10 and PCST 30/10/60 ternary systems.
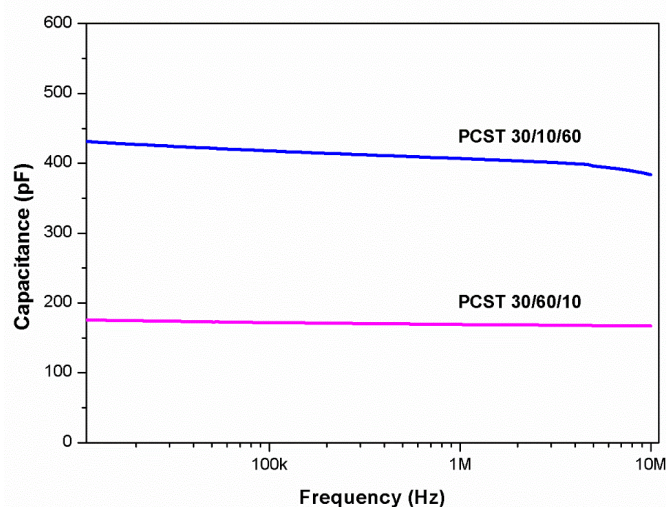

Figure 6. Dielectric capacitance of the PCST thin films prepared in O$_2$ atmosphere.

The results shown that the PCST30/10/60 thin film presents good values of dielectric capacitance, while the thin film with higher Ca^{2+} cations concentrations, the PCST 30/60/10, shows a lower value of dielectric capacitance, which causes an influence in the material's ferroelectric properties.

The curves of capacity vs. voltage (C–V curves) for the nanostructured PCST thin films are shown in Fig. 7. This graphic represents two measurements: one sweep from a negative to a positive electric field (*sweep up*), and another from the positive to negative field (*sweep down*).

For the ternary PCST30/10/60 system, the sweep up and sweep down measurement curves are symmetrical and not overlapped due to the ferroelectric nature of the thin film; however, this behavior is less pronounced than in the pure PT system. With the increase of the Ca^{2+} cations and the decreases of Sr^{2+} cations incorporation (PCST30/60/10 system), there is an overlapping of the sweep up and sweep down curves, which is a characteristic due to the non-ferroelectric nature of the material, i.e., a tendency towards a paraelectric phase

manifested by the lack of effective local and long-range polarization.
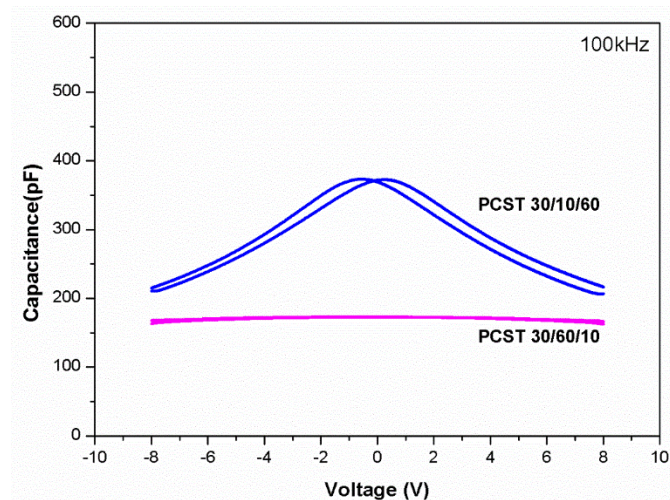
Figure 7. C−V curves for the PCST thin films prepared in O_2 atmosphere.

The phase transition of the PCST thin films was also studied by electrical characterization. Structural phase transitions are changes in crystal structure caused by changes in an order parameter, which is defined as any physical quantity describing the phase transition. In ferroelectric materials there is a temperature, called Curie temperature (T_C), in which a structural transition between the paraelectric and ferroelectric phases is observed, that is associated with a change in the material's crystalline structure to a new symmetry. An important feature of the ferroelectric phase transition is that the dielectric permittivity increases considerably at the transition temperature. Figures 8 and 9 illustrate the phase transition temperature for thin films PCST30/10/60 and PCT 30/60/10, respectively.

Figures 8 and 9 show the T_C changes as a function of the Ca^{2+} e Sr^{2+} cations concentration. The decrease of the Tc is expected since the matrix of the PCST system, PT, has a T_C ~763 K, while ST has a T_C ~105 K for a ferroelectric to paraelectric transition accompanied by a change from tetragonal to cubic structure, respectively. On the other hand, the CT presents an orthorhombic structure at room temperature and tetragonal structure at 1500 K and finally cubic structure at T_C ~1580 K. Therefore, the results confirm, once again, the strong influence of Sr^{2+} on Ca^{2+} cations and its competition within the crystal lattice of ternary PCST structure.
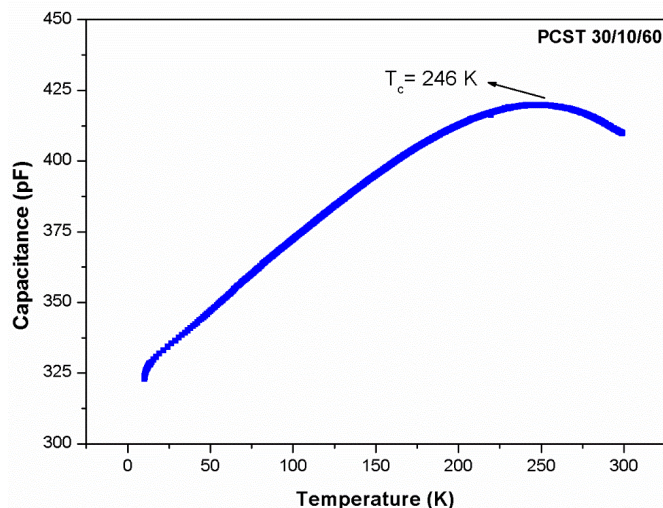

Figure 8. Dependence of capacitance as a function of temperature for PCST 30/10/60 thin film.
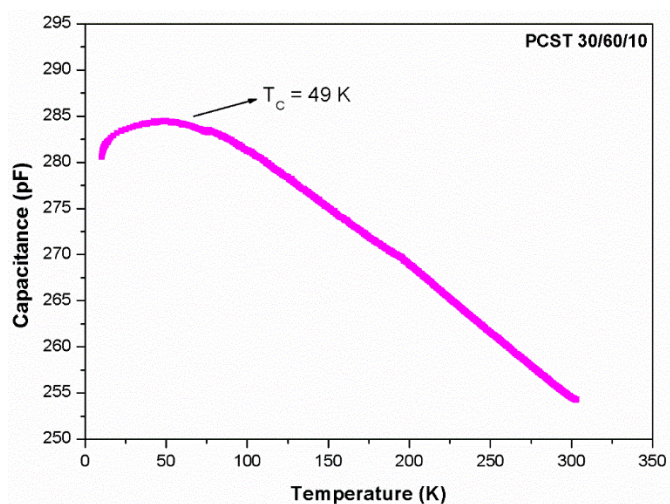
Figure 9. Dependence of capacitance as a function of temperature for PCST 30/60/10 thin film.

To check the influence of Sr^{2+} on Ca^{2+} cations in the crystal lattice of PT structure, a theoretical study of the electronic properties of the materials was performed with the analysis of the band gap value and the density of states (DOS). Figure 10 shows the DOS for the ternary PCST systems. For both systems, the contribution of Pb, Ca, and Sr to conduction band is small compared to the contribution of Ti atoms. To the valence band there is a prevailing contribution of atomic orbitals from the O atoms.
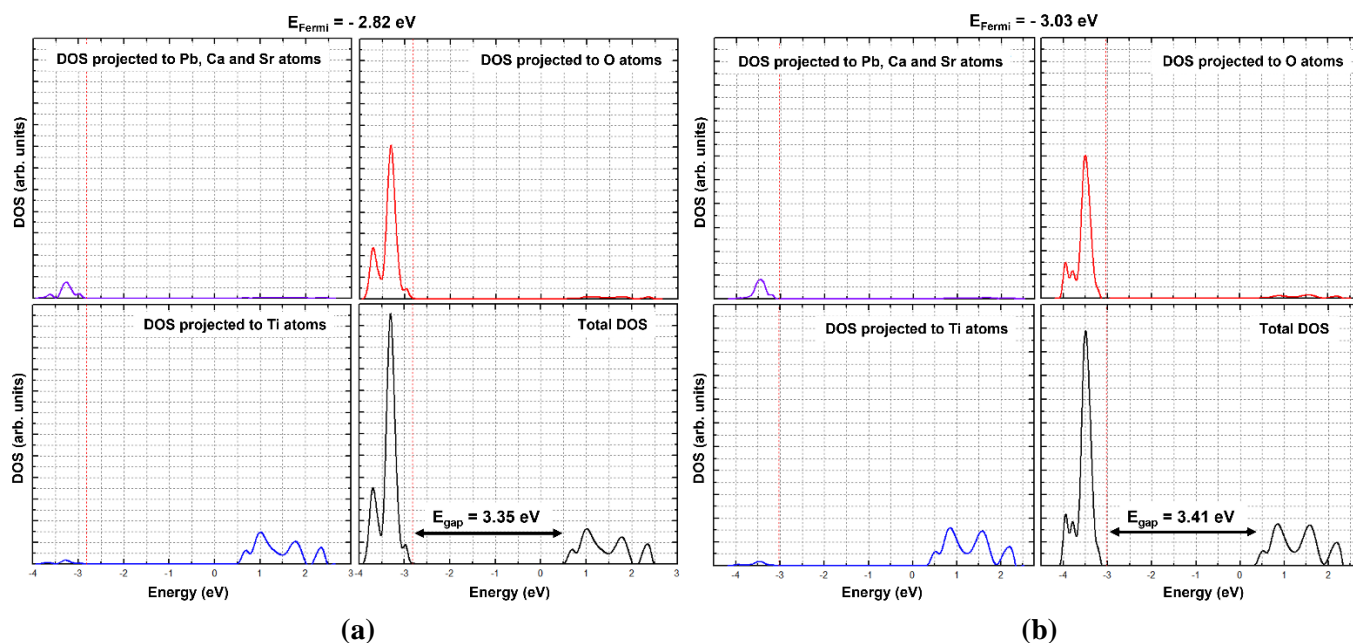
Figure 10. Total DOS: **(a)** PCST 30/10/60 and **(b)** PCST 30/60/10.

5. Conclusions

In this study, a very efficient and inexpensive chemical method to produce a good quality of ternary PCST powder and thin films were presented. In the PCST 30/10/60 and PCST 30/60/10 samples was possible to incorporate simultaneously Ca^{2+} and Sr^{2+} cations in the site AO_{12} in place of Pb^{2+} cations without phase separation, such as $PbTiO_3$, $CaTiO_3$, $SrTiO_3$, or even as complex phase $(Pb,Sr)TiO_3$ or $(Pb,Ca)TiO_3$.

The studied systems, PCST 30/60/10 and PCST 30/10/60, presented a tetragonal to cubic phase transition due to the simultaneous incorporation of Ca^{2+} and Sr^{2+} cations at low temperature, thus causing the absence of the ferroelectric nature present in PT at room temperature. The results show that this fact it was more evident in PCST 30/10/60 system, where the concentration of Sr^{2+} cations in the system is greater. These incorporations decreased the tetragonality and significantly reduced the octahedron distortion, promoting the elimination of ferroelectric character at room temperature. This elimination was confirmed in the analysis of DOS projected onto the atomic orbitals of Pb, then, Pb stopped contributing to the conduction band with $6p_z$ atomic orbitals, which is responsible by ferroelectricity.

Authors' contribution

Conceptualization: Gouveia, A. F.; Pontes, F. M. L.
Data curation: Gouveia, A. F.; Ribeiro, L. K.; Assis, M.; Pontes, F. M. L.
Formal Analysis: Gouveia, A. F.; Ribeiro, L. K.; Assis, M.; Pontes, F. M. L.
Funding acquisition: Gouveia, A. F.; Longo, E.; Pontes, F. M. L.
Investigation: Gouveia, A. F.; Pontes, F. M. L.
Methodology: Gouveia, A. F.; Ribeiro, L. K.; Assis, M.; Pontes, F. M. L.
Project administration: Gouveia, A. F.; Longo, E.; Andrés, J.; Pontes, F. M. L.
Resources: Gouveia, A. F.; Longo, E.; Andrés, J.;
Software: Gouveia, A. F.; Pontes, F. M. L.
Supervision: Longo, E.; Andrés, J.;
Validation: Gouveia, A. F.; Pontes, F. M. L.
Visualization: Gouveia, A. F.; Pontes, F. M. L.
Writing – original draft: Gouveia, A. F.; Ribeiro, L. K.; Assis, M.; Pontes, F. M. L.
Writing – review & editing: Gouveia, A. F.; Ribeiro, L. K.; Longo, E.; Andrés, J.; Pontes, F. M. L.

Data availability statement

All data sets were generated or analyzed in the current study.

Funding

Acknowledgments

References

Ahmadi, F.; Araghi, H. Electro-optical and phonon properties of $PbTiO_3/CaTiO_3/SrTiO_3$ ferroelectric superlattices: a first-principles calculation. *J. Nanophotonics* **2021**, *15* (2), 026003. https://doi.org/10.1117/1.Jnp.15.026003

Becke, A. D. Density-Functional Thermochemistry. The Role of Exact Exchange. *J. Chem. Phys.* **1993**, *98* (7), 5648–5652. https://doi.org/10.1063/1.464913

Capeli, R. A.; Pontes, F. M. L.; Chiquito, A. J.; Bastos, W. B.; Pereira-da-Silva, M. A.; Longo, E. Annealing temperature dependence of local piezoelectric response of $(Pb,Ca)TiO_3$ ferroelectric thin films. *Ceram. Int.* **2017**, *43* (6), 5047–5052. https://doi.org/10.1016/j.ceramint.2017.01.015

Crawford, J. C. Ferroelectric-Piezoelectric Random Access Memory. *IEEE Tran. Electron Devices.* **1971**, *18* (10), 951–958. https://doi.org/10.1109/T-ED.1971.17309

Daglish, M.; Kemmitt, T. Ferroelectric thin films – research, development and commercialization. *IPENZ Transactions.* **2000**, *27* (1), 21–24. https://search.informit.org/doi/abs/10.3316/INFORMIT.185207029730394 (accessed 2022-05-18).

Dovesi, R.; Orlando, R.; Civalleri, B.; Roetti, C.; Saunders, V. R.; Zicovich-Wilson, C. M. CRYSTAL: a computational tool for the *ab initio* study of the electronic properties of crystals. *Z. Kristallogr.* **2005**, *220* (5–6), 571–573. https://doi.org/10.1524/zkri.220.5.571.65065

Eshita, T.; Tamura, T.; Arimoto Y. Ferroelectric random access memory (FRAM) devices. *Advances in Non-Volatile Memory and Storage Technology.* **2014**, 434–454. https://doi.org/10.1533/9780857098092.3.434

Eshita, T.; Wang, W. S.; Nomura, K.; Nakamura, K.; Saito, H.; Yamaguchi, H.; Mihara, S.; Hikosaka, Y.; Kataoka, Y.; Kojima, M. Development of highly reliable ferroelectric random access memory and its Internet of Things applications. *Jpn. J. Appl. Phys.* **2018**, *57*, 11UA01. https://doi.org/10.7567/JJAP.57.11UA01

Han, S. T.; Zhou, Y.; Roy, V. A. L. Towards the Development of Flexible Non-Volatile Memories. *Adv. Mater.* **2013**, *25* (38), 5425–5449. https://doi.org/10.1002/adma.201301361

Kim, K.; Lee, S. Integration of lead zirconium titanate thin films for high density ferroelectric random access memory. *J. Appl. Phys.* **2006**, *100* (5), 051604. https://doi.org/10.1063/1.2337361

Kour, P.; Pradhan, S. K. Perovskite Ferroelectric. *IntechOpen.* **2021**. https://doi.org/10.5772/intechopen.98382

Lázaro, S. R. D.; Longo, E.; Beltran, A.; Sambrano, J. R. Propriedades eletrônicas e estruturais do $PbTiO_3$: teoria do funcional de densidade aplicada a modelos periódicos theory applied to periodic models. *Quim. Nova.* **2005**, *28* (1), 10–18. https://doi.org/10.1590/S0100-40422005000100003

Leal, S. H.; Pontes, F. M. L.; Leite, E. R.; Longo, E.; Pizani, P. S.; Chiquito, A. J.; Machado, M. A. C.; Varela, J. A. Ferroelectric phase transition in $Pb_{0.60}Sr_{0.40}TiO_3$ thin films. *Mater. Chem. Phys.* **2004**, *87* (2–3), 353–356. https://doi.org/10.1016/j.matchemphys.2004.05.032

Lee, C. T.; Yang, W. T.; Parr, R. G. Development of the Colle-Salvetti Correlation-Energy Formula into a Functional of the Electron-Density. *Phys. Rev. B.* **1988**, *37*, 785–789. https://doi.org/10.1103/PhysRevB.37.785

Lee, J. D. *Química Inorgânica não tão concisa*. Blucher-São Paulo, 1999.

Ling, Q.-D.; Chang, F.-C.; Song, Y.; Zhu, C.-X.; Liaw, D.-J.; Chan, D. S.-H.; Kang, E.-T.; Neoh, K.-G. Synthesis and dynamic random access memory behavior of a functional polyimide. *J. Amer. Chem. Soc.* **2006**, *128* (27), 8732–8733. https://doi.org/10.1021/ja062489n

Liu, X. D.; Zhang, D. C.; Zhang, Y.; Dai, X. T. Preparation and characterization of p-type semiconducting tin oxide thin film gas sensors. *J. Appl. Phys.* **2010**, *107* (6), 064309. https://doi.org/10.1063/1.3354092

Longo, E.; Orhan, E.; Pontes, F. M. L.; Pinheiro, C. D.; Leite, E. R.; Varela, J. A.; Pizani, P. S.; Boschi, T. M.; Lanciotti, F.; Beltrán, A.; Andrés, J. Density functional theory calculation

of the electronic structure of $Ba_{0.5}Sr_{0.5}TiO_3$:Photoluminescent properties and structural disorder. *Phys. Rev. B.* **2004**, *69*, 125115. https://doi.org/10.1103/PhysRevB.69.125115

Mao, D.; Mejia, I.; Salas-Villasenor, A. L.; Singh, M.; Stiegler, H.; Gnade, B. E.; Quevedo-Lopez, M. A. Ferroelectric random access memory based on one-transistor-one-capacitor structure for flexible electronics. *Org. Electron.* **2013**, *14* (2), 505–510. https://doi.org/10.1016/j.orgel.2012.10.035

Muller, G.; Nagel, N.; Pinnowa, C. U.; Rohr, T. *Emerging non-volatile memory technologies*. 29th European Solid-State Circuits Conference. Estoril, Portugal, 2003.

Pontes, D. S. L.; Leite, E. R.; Pontes, F. M. L.; Longo, E.; Varela, J. A. Microstructural, dielectric and ferroelectric properties of calcium-modified lead titanate thin films derived by chemical processes. *J. Eur. Ceram. Soc.* **2001a**, *21* (8), 1107–1114. https://doi.org/10.1016/S0955-2219(00)00307-1

Pontes, D. S. L.; Leite, E. R.; Pontes, F. M. L.; Longo, E.; Varela, J. A. Preparation and properties of ferroelectric $Pb_{1-x}Ca_xTiO_3$ thin films produced by the polymeric precursor method. *Journal of Materials Science.* **2001b**, *36* (14), 3461–3466. https://doi.org/10.1023/A:1017916213489

Pontes, F. M. L.; Leite, E. R.; Pontes, D. S. L.; Longo, E.; Santos, E. M. S.; Mergulhao, S.; Pizani, P. S.; Lanciotti, F.; Boschi, T. M.; Varela, J. A. Ferroelectric and optical properties of $Ba_{0.8}Sr_{0.2}TiO_3$ thin film. *J. Appl. Phys.* **2002**, *91* (9), 5972–5978. https://doi.org/10.1063/1.1466526

Pontes, F. M. L.; Pontes, D. S. L.; Leite, E. R.; Longo, E.; Santos, E. M. S.; Mergulhao, S.; Varela, J. A. Synthesis, ferroelectric and optical properties of (Pb,Ca)TiO_3 thin films by soft solution processing. *J. Sol-Gel Sci. Technol.* **2003**, *27* (2), 137–147. https://doi.org/10.1023/A:1023742315962

Pontes, F. M. L.; Pontes, D. S. L.; Leite, E. R.; Longo, E.; Chiquito, A. J.; Machado, M. A. C.; Pizani, P. S.; Varela, J. A. A Raman and dielectric study of a diffuse phase transition in $(Pb_{1-x}Ca_x)TiO_3$ thin films. *Appl. Phys. A.* **2004**, *78* (3), 349–354. https://doi.org/10.1007/s00339-003-2287-1

Pontes, F. M. L.; Leal, S. H.; Leite, E. R.; Longo, E.; Pizani, P. S.; Chiquito, A. J.; Machado, M. A. C.; Varela, J. A. Absence of relaxor-like ferroelectric phase transition in (Pb,Sr)TiO_3 thin films. *Appl. Phys. A.* **2005**, *80* (4), 813–817. https://doi.org/10.1007/s00339-003-2490-0

Pontes, F. M. L.; Galhiane, M. S.; Santos, L. S.; Rissato, S. R.; Pontes, D. S. L.; Longo E.; Leite, E. R.; Chiquito, A. J.; Pizani, P. S.; Jardim, R. F.; Escote, M. T. Pressure-induced electrical and structural anomalies in $Pb_{1-x}Ca_xTiO_3$ thin films grown at various oxygen pressures by chemical solution route. *J. Phys. D: Appl. Phys.* **2008**, *41* (11), 115402. https://doi.org/10.1088/0022-3727/41/11/115402

Pontes, D. S. L.; Pontes, F. M. L.; Capeli, R. A.; Garzim, M. L.; Chiquito, A. J.; Longo, E. Structural, ferroelectric, and optical properties of $Pb_{0.60}Ca_{0.20}Sr_{0.20}TiO_3$, $Pb_{0.50}Ca_{0.25}Sr_{0.25}TiO_3$ and $Pb_{0.40}Ca_{0.30}Sr_{0.30}TiO_3$ thin films prepared by the chemical solution deposition technique. *Ceram. Int.* **2014**, *40* (8 Part B), 13363–13370. https://doi.org/10.1016/j.ceramint.2014.05.052

Souza, R. A. Transport properties of dislocations in $SrTiO_3$ and other perovskites. *Curr. Opin. Solid State Mater. Sci.* **2021**, *25* (4), 100923. https://doi.org/10.1016/j.cossms.2021.100923

Vopson, M. M.; Tan, X. Four-State Anti-Ferroelectric Random Access Memory. *IEEE Electron Device Lett.* **2016**, *37* (12), 1551–1554. https://doi.org/10.1109/LED.2016.2614841

XCrySDen. *X-window CRYstalline Structures and DENsities*. 2019. http://www.xcrysden.org/ (accessed 2022-05-18).

Yang, C.; Xu, X. J.; Ali, W.; Wang, Y. J.; Wang, Y. P.; Yang, Y.; Chen, L.; Yuan, G. L. Piezoelectricity in Excess of 800 pC/N over 400 °C in $BiScO_3$-$PbTiO_3$-$CaTiO_3$ Ceramics. *ACS Appl. Mater. Interfaces.* **2021**, *13* (28), 33253–33261. https://doi.org/10.1021/acsami.1c07492

Yang, Y. H.; Wu, M.; Li, X. F.; Hu, H. H.; Jiang, Z. Z.; Li, Z.; Hao, X. T.; Zheng, C. Y.; Lou, X. J.; Pennycook, S. J.; Wen, Z. The Role of Ferroelectric Polarization in Resistive Memory Properties of Metal/Insulator/Semiconductor Tunnel Junctions: A Comparative Study. *ACS Appl. Mater. Interfaces.* **2020**, *12* (29), 32935–32942. https://doi.org/10.1021/acsami.0c08708

Yuan, H.; Li, L.; Hong, H.; Ying, Z.; Zheng, X.; Zhang, L.; Wen, F.; Xu, Z.; Wu, W.; Wang, G. Low sintering temperature, large strain and reduced strain hysteresis of $BiFeO_3$–$BaTiO_3$ ceramics for piezoelectric multilayer actuator applications. *Ceram. Int.* **2021**, *47* (22), 31349–31356. https://doi.org/10.1016/j.ceramint.2021.08.008

Zhang, S.; Li, Z.; Zhang, M.; Zhang, D.; Yan, Y. Enhanced piezoelectric properties of PYN-PHT ceramics by LiF addition in low temperature sintering. *J. Alloys Compd.* **2022**, *889*, 161649. https://doi.org/10.1016/j.jallcom.2021.161649

Zhao, T.-L.; Bokov, A. A.; Wu, J. G.; Wang, H. L.; Wang, C.-M.; Yu, Y.; Wang, C.-L.; Zeng, K. Y.; Ye, Z.-G.; Dong, S. X. Giant Piezoelectricity of Ternary Perovskite Ceramics at High Temperatures. *Adv. Funct. Mater.* **2019**, *29* (12), 1807920. https://doi.org/10.1002/adfm.201807920